Mechanical, elastic, anisotropy, and electronic properties of monoclinic phase of m-$Si_xGe_{3-x}N_4$*

Zhen-Yang Ma(马振洋)†, Fang Yan(阎芳), Su-Xin Wang(王苏鑫), Qiong-Qiong Jia(贾琼琼), Xin-Hai Yu(于新海), and Chun-Lei Shi(史春蕾)

Tianjin Key Laboratory for Civil Aircraft Airworthiness and Maintenance, Civil Aviation University of China, Tianjin 300300, *China*

(Received 8 August 2017; revised manuscript received 6 September 2017; published online 20 November 2017)

The structural, mechanical, elastic anisotropic, and electronic properties of the monoclinic phase of m-Si_3N_4, m-Si_2GeN_4, m-$SiGe_2N_4$, and m-Ge_3N_4 are systematically investigated in this work. The calculated results of lattice parameters, elastic constants and elastic moduli of m-Si_3N_4 and m-Ge_3N_4 are in good agreement with previous theoretical results. Using the Voigt–Reuss–Hill method, elastic properties such as bulk modulus B and shear modulus G are investigated. The calculated ratio of B/G and Poisson's ratio v show that only m-$SiGe_2N_4$ should belong to a ductile material in nature. In addition, m-$SiGe_2N_4$ possesses the largest anisotropic shear modulus, Young's modulus, Poisson's ratio, and percentage of elastic anisotropies for bulk modulus A_B and shear modulus A_G, and universal anisotropic index A_U among m-$Si_xGe_{3-x}N_4$ ($x = 0$, 1, 2, 3.) The results of electronic band gap reveal that m-Si_3N_4, m-Si_2GeN_4, m-$SiGe_2N_4$, and m-Ge_3N_4 are all direct and wide band gap semiconducting materials.

Keywords: $Si_xGe_{3-x}N_4$, mechanical properties, elastic anisotropic, electronic properties

PACS: 61.50.–f, 61.50.Ah, 71.20.Nr, 71.55.Cn **DOI:** 10.1088/1674-1056/26/12/126105

1. Introduction

Nitrides consisting of III A and IV A group elements can be used as high temperature materials, catalysts, light-emitting diodes and refractory ceramics because of their excellent mechanical and thermodynamic properties.[1–4] Silicon nitride is an important ceramic material. It is a superhard material and atomic crystal which has good lubricity and abrasion resistance. It resists oxidation at high temperature, and it can resist cold and hot shocks, it can be heated to over 1000 K in the air and will not be broken by rapid cooling and rapid heating. Because silicon nitride ceramic has such excellent characteristics, it is often used in bearings, gas turbine blades, mechanical seals, permanent die, and other mechanical components. If the silicon nitride ceramic with high temperature resistance and high heat transfer resistance is used to make the heating surfaces of the engine parts, it can not only improve the quality of diesel engine, save fuel, but also enhance the thermal efficiency. In fact, germanium is adopted because Ge atoms have higher carrier mobility than Si atoms. The semiconductor field effect transistor has superior performances. The germanium atom radius is bigger, so the critical pressure of the phase transition of Ge_3N_4 is less than that of Si_3N_4. Germanium nitride also has the advantages of corrosion resistance, high hardness, and its band gap can be adjusted. Many new structures of silicon nitride and germanium nitride have been reported in many researches.[5–8] It has been known for several decades that silicon nitride exists in two stable phases (namely α- and β-Si_3N_4) with very similar structures,[5] they both have hexagonal symmetry. The phase boundaries of the $\beta \rightarrow$P-6$' \rightarrow \delta$ transitions are investigated using first-principles calculations within the quasi-harmonic approximation by Yu and Chen.[6] Using the plane-wave pseudopotential method, Yu and Chen[7] have investigated the structural properties, mechanical properties and thermodynamic properties of β-, γ-, wII-, and post-spinel Si_3N_4 and also the phase transition characters among these polymorphs. Wang *et al.* have conducted a comparative structural and electronic study of a new class of material, olivine-Si_3N_4 and olivine-Ge_3N_4 by using the first principles approach.[8] They found that olivine-Si_3N_4 has a large bulk modulus (262.9 GPa), and olivine-Si_3N_4 and olivine-Ge_3N_4 are both direct bang gap semiconductors with the band gaps of 2.99 eV and 1.55 eV, respectively.

The structural, electronic, and optical properties of the new cubic spinel nitrides c-Si_3N_4, c-$SiGe_2N_4$, c-Si_2GeN_4, and c-Ge_3N_4 were studied by a first-principles method.[9] The c-$SiGe_2N_4$ is a direct band gap semiconductor with a band gap of 1.85 eV, and the c-Si_2GeN_4 is an indirect band gap semiconductor with a band gap of 2.56 eV. In addition, the bulk moduli of c-$SiGe_2N_4$ and c-Si_2GeN_4 are 277.1 GPa and 258.3 GPa, respectively. Using first-principles calculations, the structural, electronic, elastic, and optical properties of cubic spinel $SiGe_2N_4$ under pressure were investigated by Moakafi *et al.*[10] Bouhemadou *et al.*[11] have investigated the structural, elastic, electronic, optical and thermal properties of c-$SiGe_2N_4$ by using the ultrasoft pseudopotential density functional method in the generalized gradient approximation under

*Project supported by the National Natural Science Foundation of China (Grant No. 61601468), the Fundamental Research Funds for the Central Universities, China (Grant No. 3122014C024), and the Fund for Scholars of Civil Aviation University of China (Grant No. 2013QD06X).

†Corresponding author. E-mail: zyma@cauc.edu.cn

© 2017 Chinese Physical Society and IOP Publishing Ltd

pressure. The structural and mechanical properties of the cubic spinel c-CSi_2N_4 were studied by first-principles total energy calculations based on the density-functional theory.[12] The Vickers hardness of c-CSi_2N_4 is 52.07 GPa, so it is a potential superhard material. Cui *et al*. explored three Si_3N_4 metastable phases, i.e., tetragonal t-Si_3N_4, monoclinic m-Si_3N_4 and orthorhombic o-Si_3N_4, by analyzing the crystal structure obtained through using the particle swarm optimization (CALYPSO) code.[13] The m-Si_3N_4 belongs to the space group of *Cm* in a monoclinic system and it is mechanically and dynamically stable under ambient pressure based on their elastic constants and phonon dispersions calculations. Cang *et al*. predicted the lattice structures, densities of states, phonon dispersion curves of m-, t-, and o-Ge_3N_4.[14] The stabilities of these Ge_3N_4 structures were verified by the proving of negative formation enthalpy, the satisfying of Born's stability criteria and no imaginary frequency in the phonon dispersion curves in a pressure range of 0 GPa–20 GPa. Fan *et al*. investigated the electronic structures, elastic, anisotropic, and electronic properties of m-Si_3N_4, t-Si_3N_4, and o-Si_3N_4 under pressure,[15] and it is interesting that the shift of band gap from direct to indirect occurs for m-Si_3N_4 when the pressure rises up to 50 GPa. Chen *et al*.[16] predicted the structural, electronic, optical and thermodynamic properties of m-, t-, and o-M_3N_4 (M = Si, Ge, Sn).

According to the previous work, we predict two new double nitrides m-Si_2GeN_4 and m-$SiGe_2N_4$ in the *Cm* space group. In the present work, the structural, elastic anisotropic, and electronic properties of m-Si_3N_4, m-Si_2GeN_4, m-$SiGe_2N_4$, and m-Ge_3N_4 are investigated using density functional theory calculations. The Debye temperature, the ductile or brittle characters and elastic anisotropy of m-$Si_xGe_{3-x}N_4$ ($x = 0$, 1, 2, 3.) are discussed in detail.

2. Computational details and theory

The structural optimizations and property predictions of the monoclinic structures of m-$Si_xGe_{3-x}N_4$ (x = 0, 1, 2, 3) were performed based on density functional theory (DFT)[17,18] as implemented in the Cambridge Serial Total Energy Package (CASTEP) code.[19] The exchange–correlation potential was treated with the generalized gradient approximation (GGA) in the form of Perdew–Burke–Ernzerhof (PBE),[20] PBE for solid (PBEsol),[21] and the local density approximation (LDA) in the form of Ceperley and Alder data parameterized by Perdew and Zunger (CA-PZ).[22,23] The Broyden–Fletcher–Goldfarb–Shanno (BFGS)[24] minimization scheme was used in geometry optimization. Vanderbilt type ultrasoft pseudopotentials[25] were employed to describe the interactions between ionic core and valence electrons. The considered valence atomic configurations had been set to be Si-$3s^23p^2$, Ge-$4s^24p^2$, and N-$2s^22p^3$. In the structure calculation, a plane-wave basis set with energy cut-off 500 eV was used for all cases. The k-points of $6\times14\times7$, $6\times13\times7$, $6\times13\times7$, and $5\times13\times7$ were adopted for the structures of m-Si_3N_4, m-Si_2GeN_4, m-$SiGe_2N_4$, and m-Ge_3N_4 by using Monkhorst–Pack mesh,[26] respectively. The system reached the ground state via self-consistent calculation when the total energy, the maximum displacement of ion, the maximum ionic Hellmann–Feynman force within and the maximum stress were less than 5×10^{-6} eV/atom, 5×10^{-4} Å, 0.01 eV/Å, and 0.02 GPa, respectively. In order to calculate electronic structures, the HSE06 hybrid functional[27] was used.

3. Results and discussion

The crystal structures of m-Si_3N_4 and the double nitrides m-Si_2GeN_4 and m-$SiGe_2N_4$ are shown in Fig. 1. In a conventional cell, m-Si_3N_4 (m-Ge_3N_4) has 8 N atoms and 6 Si (Ge) atoms. For m-Si_2GeN_4 and m-$SiGe_2N_4$, the Ge atoms replace Si atoms with the smallest energy. The equilibrium lattice constants are determined by the minimum total energy with respect to the variation of the cell volume through utilizing both GGA and LDA. The optimized lattice parameters of m-Si_3N_4, m-Si_2GeN_4, m-$SiGe_2N_4$, and m-Ge_3N_4 at zero pressure are listed in Table 1.

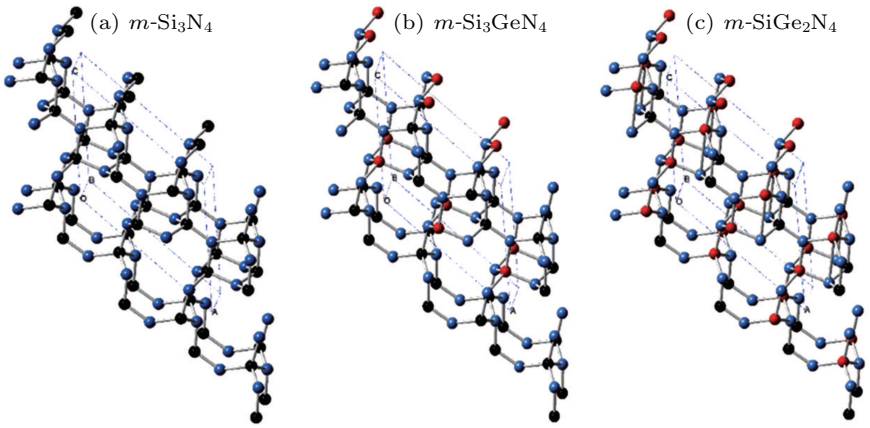


Fig. 1. (color online) Crystal structures of (a) m-Si_3N_4 , (b) m-Si_2GeN_4, and (c) m-Ge_3N_4 under ambient pressure. The silicon, germanium, and nitrogen atoms are represented as black, red, and blue spheres, respectively.

Table 1. Calculated lattice parameters (a, b, c in unit Å and β in unit degree) of m-Si_3N_4, m-Si_2GeN_4, m-$SiGe_2N_4$, and m-Ge_3N_4 compared with previous theoretical results.

Materials	PBE				PBEsol				CA-PZ			
	a	b	c	β	a	b	c	β	a	b	c	β
m-Si_3N_4	9.606	2.932	7.419	133.3	9.590	2.928	7.409	133.6	9.442	2.888	7.308	133.6
	9.512[a]	2.904	7.353	133.4								
	9.605[b]	2.933	7.417	133.4								
	9.603[c]	2.932	7.419									
m-Si_2GeN_4	9.754	2.989	7.569	132.8	9.735	2.983	7.551	132.8	9.558	2.933	7.422	133.0
m-$SiGe_2N_4$	9.896	3.043	7.787	132.8	9.876	3.036	7.770	132.8	9.672	2.975	7.603	133.1
m-Ge_3N_4	10.218	3.104	7.931	133.6	10.188	3.095	7.913	133.6	9.924	3.021	7.714	133.7
	10.215[d]	3.103	7.928									

[a] Ref. [13], [b] Ref. [15], [c] Ref. [16], [d] Ref. [14].

Along with previous theoretical results for comparison, it can be seen that the calculated lattice parameters of m-Si_3N_4 and m-Ge_3N_4 are in excellent agreement with previous results.[13,15,16] The variations of the lattice parameters (a, b, c) with increasing the composition of germanium are shown in Fig. 2. On the whole, the lattice parameters (a, b, c) increase with increasing the composition of germanium. The augment tendency of lattice parameter b is nearly linear while the lattice parameter a and c increases nonlinearly with increasing the composition of germanium. The curves of the PBE and PBEsol methods almost coincide as shown in Fig. 2. From m-Si_3N_4 to m-Ge_3N_4, the lattice parameters a, b, and c increase by 6.34% (5.10%), 5.87% (4.61%), and 6.90% (5.56%) obtained from the PBE (CA-PZ) method, respectively.

The elastic constants are closely related to various fundamental mechanical properties of a crystal, which can provide, particularly, the information about the stability and stiffness of materials. For a monoclinic crystal, there are thirteen independent elastic constants, namely C_{11}, C_{22}, C_{33}, C_{44}, C_{55}, C_{66}, C_{12}, C_{13}, C_{15}, C_{23}, C_{25}, C_{35}, and C_{46}. The calculated elastic constants of m-$Si_xGe_{3-x}N_4$ ($x = 0$, 1, 2, 3) are listed in Table 2. The elastic constants of m-Si_3N_4 and m-Ge_3N_4 are well consistent with pervious theoretical values.[13,14] For a stable crystal of monoclinic structure, it must obey the following mechanical stability according to the Born's criteria:[28]

$$C_{ii} > 0 \quad (i = 1\text{–}6), \tag{1}$$

$$C_{11} + C_{22} + C_{33} + 2(C_{12} + C_{13} + C_{23}) > 0, \tag{2}$$

$$C_{33}C_{55} - C_{35}^2 > 0, \tag{3}$$

$$C_{44}C_{66} - C_{46}^2 > 0, \tag{4}$$

$$C_{22} + C_{33} - 2C_{23} > 0, \tag{5}$$

$$C_{22}\left(C_{33}C_{55} - C_{35}^2\right) + 2C_{23}C_{25}C_{35} - C_{23}^2C_{55} - C_{25}^2C_{33} > 0, \tag{6}$$

$$\begin{aligned} &2[C_{15}C_{25}(C_{33}C_{12} - C_{13}C_{23}) + C_{15}C_{35}(C_{22}C_{13} - C_{12}C_{23}) \\ &+ C_{25}C_{35}(C_{11}C_{23} - C_{12}C_{13})] \\ &- [C_{15}^2\left(C_{22}C_{33} - C_{23}^2\right) + C_{25}^2\left(C_{11}C_{33} - C_{13}^2\right) \\ &+ C_{35}^2\left(C_{11}C_{22} - C_{12}^2\right)] + gC_{55} > 0, \end{aligned} \tag{7}$$

$$g = C_{11}C_{22}C_{33} - C_{11}C_{23}^2 - C_{22}C_{13}^2 - C_{33}C_{12}^2 + 2C_{12}C_{13}C_{23}. \tag{8}$$

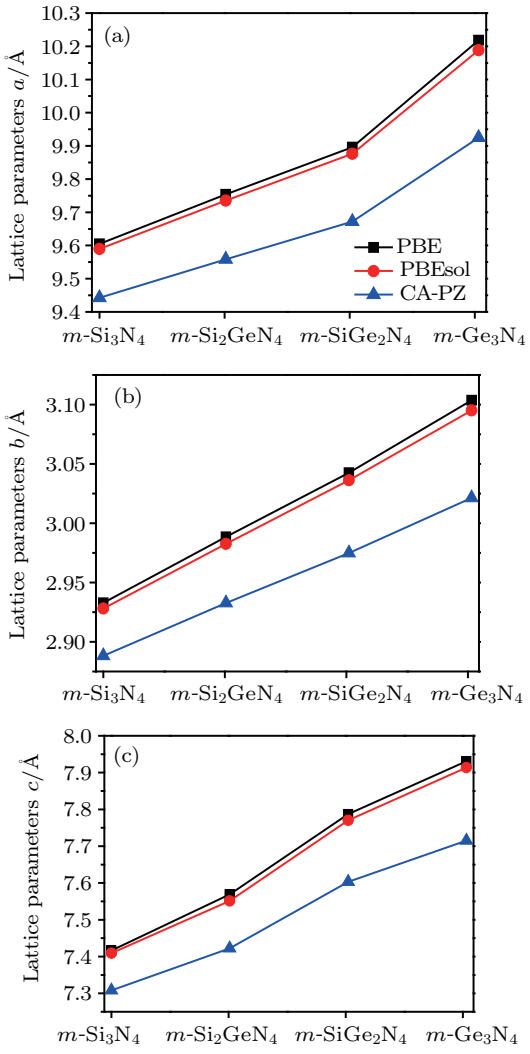


Fig. 2. (color online) Calculated lattice parameters ((a) a, (b) b, and (c) c) of m-Si_3N_4, m-Si_2GeN_4, m-$SiGe_2N_4$, and m-Ge_3N_4 by PBE, PBEsol, and CA-PZ methods.

It can be easily verified that the elastic constants of m-$Si_xGe_{3-x}N_4$ ($x = 0$, 1, 2, 3) satisfy their stability requirements, which indicates that they are mechanical stable. And the dynamic stabilities of m-Si_3N_4 and m-Ge_3N_4 have been verified by the phonon spectrum calculations in Refs. [13] and [14].

So it is revealed that m-Si_3N_4 and m-Ge_3N_4 are mechanically and dynamically stable via the elastic constants and phonon calculations. The elastic constants C_{11}, C_{22}, C_{33} represent the stiffness of the material when applying stresses along the x, y, z directions,[29] respectively. The obtained result obviously shows that all the m-Si_3N_4, m-Si_2GeN_4, m-$SiGe_2N_4$, and m-Ge_3N_4 follow this ordering relationship: $C_{22} > C_{33} > C_{11}$, which means that the resistance against deformation along the z axis is stronger than along the x axis but weaker than along the y axis. Simultaneously, with increasing the components of Ge atoms, the elastic constants C_{ii} decrease, and thus the compression property increases.

Table 2. Calculated elastic constants (in unit GPa) of m-Si_3N_4, m-Si_2GeN_4, m-$SiGe_2N_4$, and m-Ge_3N_4 compared with other calculated results.

	C_{11}	C_{22}	C_{33}	C_{44}	C_{55}	C_{66}	C_{12}	C_{13}	C_{15}	C_{23}	C_{25}	C_{35}	C_{46}
m-Si_3N_4	257	455	353	93	132	92	36	131	–27	58	22	16	30
	254[a]	478	369	70	130	95	40	142		57	23	18	34
m-Si_2GeN_4	242	417	316	76	112	85	37	126	–18	53	16	15	22
m-$SiGe_2N_4$	235	436	363	60	110	42	42	164	–30	68	20	21	19
m-Ge_3N_4	180	344	274	57	90	61	34	110	–18	40	9	19	22
	175[b]	338	277	55	90	63	31	107		41	9.8	20	22

[a] Ref. [13], [b] Ref. [14].

Furthermore, according to the Voigt–Reuss–Hill (VRH) average scheme,[30,31] the bulk modulus B and shear modulus G can be estimated using calculated elastic constants via the following equations:

$$B_{\mathrm{V}} = (1/9)\left[C_{11}+C_{22}+C_{33}+2\left(C_{12}+C_{13}+C_{23}\right)\right], \tag{9}$$

$$\begin{aligned} B_{\mathrm{R}} = {} & \Omega\left[a\left(C_{11}+C_{22}-2C_{12}\right)+b\left(2C_{12}-2C_{11}-C_{23}\right)\right. \\ & +c\left(C_{15}-2C_{25}\right)+d\left(2C_{12}+2C_{23}-C_{13}-2C_{22}\right) \\ & \left.+2e\left(C_{25}-C_{15}\right)+f\right]^{-1}, \end{aligned} \tag{10}$$

$$\begin{aligned} G_{\mathrm{V}} = {} & (1/15)\left[C_{11}+C_{22}+C_{33}+3\left(C_{44}+C_{55}+C_{66}\right)\right. \\ & \left.-\left(C_{12}+C_{13}+C_{23}\right)\right], \end{aligned} \tag{11}$$

$$\begin{aligned} G_{\mathrm{R}} = {} & 15\left\{4\left[a\left(C_{11}+C_{22}+C_{33}\right)+b\left(C_{11}-C_{12}-C_{23}\right)\right.\right. \\ & +c\left(C_{15}+C_{25}\right)+d\left(C_{22}-C_{12}-C_{23}-C_{13}\right) \\ & \left.+e\left(C_{15}-C_{25}\right)+f\right]/\Omega \\ & \left.+3\left[g/\Omega+\left(C_{44}+C_{66}\right)/\left(C_{44}C_{66}-C_{46}^2\right)\right]\right\}^{-1}, \end{aligned} \tag{12}$$

$$a = C_{33}C_{55}-C_{35}^2, \tag{13}$$

$$b = C_{23}C_{55}-C_{25}C_{35}, \tag{14}$$

$$c = C_{13}C_{35}-C_{15}C_{33}, \tag{15}$$

$$d = C_{13}C_{55}-C_{15}C_{35}, \tag{16}$$

$$e = C_{13}C_{25}-C_{15}C_{23}, \tag{17}$$

$$\begin{aligned} f = {} & C_{11}\left(C_{22}C_{55}-C_{25}^2\right)-C_{12}\left(C_{12}C_{55}-C_{15}C_{25}\right) \\ & +C_{15}\left(C_{12}C_{25}-C_{15}C_{25}\right) \\ & +C_{25}\left(C_{23}C_{35}-C_{25}C_{33}\right), \end{aligned} \tag{18}$$

$$\begin{aligned} \Omega = {} & 2\left[C_{15}C_{25}\left(C_{33}C_{12}-C_{13}C_{23}\right)\right. \\ & +C_{15}C_{35}\left(C_{22}C_{13}-C_{12}C_{23}\right) \\ & \left.+C_{25}C_{35}\left(C_{11}C_{23}-C_{12}C_{13}\right)\right]-\left[C_{15}^2\left(C_{22}C_{33}-C_{23}^2\right)\right. \\ & \left.+C_{25}^2\left(C_{11}C_{33}-C_{13}^2\right)+C_{35}^2\left(C_{11}C_{22}-C_{12}^2\right)\right] \\ & +gC_{55}, \end{aligned} \tag{19}$$

$$B = \frac{1}{2}\left(B_{\mathrm{V}}+B_{\mathrm{R}}\right), \quad G = \frac{1}{2}\left(G_{\mathrm{V}}+G_{\mathrm{R}}\right). \tag{20}$$

The Young's modulus E and Poisson's ratio v are obtained from the following equations: $E = 9BG/(3B+G)$ and $v = (3B-2G)/[2(3B+G)]$, respectively. Comparing with the previous results,[13,14,16] the calculated values of bulk modulus B, shear modulus G, and Young's modulus E are presented in Table 3. The bulk modulus B represents the resistance to fracture while the shear modulus G represents the resistance to plastic deformation.[32] The values of shear modulus are much larger than those of bulk modulus for m-$Si_xGe_{3-x}N_4$ ($x = 0$, 1, 2, 3), which means that the resistance to shape change is better than that to volume change. Generally, Young's modulus E provides a measure of material stiffness. The larger the value of E, the stiffer the material will be.[33] The values of B, G, and E decrease with the increase of the Ge atoms except m-$SiGe_2N_4$, which suggests that the resistance to deformation becomes weaker and the stiffness decreases.

Table 3. Calculated values of elastic modulus (in unit GPa), Poisson's ratio v, percent compressibility of bulk modulus and shear modulus factors A_{B}, A_{G}, and anisotropic index A_{U} for m-Si_3N_4, m-Si_2GeN_4, m-$SiGe_2N_4$, and m-Ge_3N_4, compared with other calculated results.

Materials	B_{V}	B_{R}	G_{V}	G_{R}	B	G	E	B/G	v	A_{B}	A_{G}	A_{U}
	168	163	119	101	165	110	270	1.505	0.228	1.663	8.545	0.968
m-Si_3N_4					165[a]	113	276	1.457	0.220			
					165[b]	104	259	1.586	0.239			
m-Si_2GeN_4	156	152	105	89	154	97	241	1.586	0.239	1.204	8.097	0.905
m-$SiGe_2N_4$	176	165	93	62	170	78	202	2.200	0.303	3.131	19.949	2.557
m-Ge_3N_4	129	124	82	64	126	73	184	1.732	0.258	2.287	12.788	1.513
					124[c]	73						

[a] Ref. [13]. [b] Ref. [16]. [c] Ref. [14].

Poisson's ratio v can be used as an indicator for ductility or brittleness. According to the Frantsevich's rule,[34] the critical value that distinguishes between the ductile and brittle nature of material is 0.26. If $v > 0.26$, the material will behave in a ductile manner, otherwise the material demonstrates brittleness in nature. Additionally, the ratio of bulk modules to shear modulus (B/G) can also judge whether a material would be a ductile or brittle manner according to the Pugh's criterion.[35] The critical value of this ratio which distinguishes between the ductility and brittle is 1.75. For ductile materials, the ratio of B/G is larger than 1.75. Here the calculation Poisson's ratio v and ratio of B/G of m-$Si_xGe_{3-x}N_4$ ($x = 0$, 1, 2, 3) are listed in Table 3. Only the Poisson's ratio v (B/G) of m-$SiGe_2N_4$ is larger than 0.26 (1.75), meaning that m-$SiGe_2N_4$ is ductile and m-Si_3N_4, m-Si_2GeN_4, and m-Ge_3N_4 are brittle in nature. The brittle materials are sensitive to thermal shocks, as the material cannot efficiently dissipate thermal stresses via plastic deformations. Thus, a brittle material can suffer limited thermal shocks before its strength drops dramatically. Hence, the capability of resisting thermal shocks for m-$SiGe_2N_4$ is stronger than for m-Si_3N_4, m-Si_2GeN_4, and m-Ge_3N_4.

The Debye temperature (Θ_D) is one of fundamental parameters for solid materials, which is related to many physical properties, such as thermal expansion and specific heat. It is the Debye temperature that reflects the temperature of a crystal's normal mode of vibration. The Debye temperature can be estimated from averaged sound velocity (v_m), compressional sound velocity (v_p) and shear sound velocity (v_s) through the following formulas:[36,37]

$$\Theta_D = \frac{h}{k_B}\left[\frac{3n}{4\pi}\left(\frac{N_A\rho}{M}\right)\right]^{1/3} v_m, \tag{21}$$

$$v_m = \left[\frac{1}{3}\left(\frac{2}{v_p^3}+\frac{1}{v_s^3}\right)\right]^{-1/3}, \tag{22}$$

$$v_p = \left[\left(B+\frac{4G}{3}\right)/\rho\right]^{1/2}, \quad v_s = \sqrt{G/\rho}, \tag{23}$$

where h is the Planck's constant, k_B is the Boltzmann constant, N_A is the Avogadro's constant, M is the molecular weight, n is the number of atoms in the molecule, and ρ is the density of crystal. The calculated results of density, the Debye temperature and the sound velocities for m-$Si_xGe_{3-x}N_4$ ($x = 0$, 1, 2, 3) are listed in Table 4 at 0 GPa and 0 K. Following the sequence m-$Si_3N_4 \rightarrow m{-}Si_2GeN_4 \rightarrow m{-}SiGe_2N_4 \rightarrow m{-}Ge_3N_4$, the densities increase whereas the Debye temperature Θ_D and the sound velocities decrease. According to Refs. [38]–[40], a larger Θ_D suggests a higher normal vibration, which is associated with a better thermal conductivity. Meanwhile, the Debye temperature can characterize the strength of covalent bond for solid. The larger the Θ_D, the stronger the covalent bond is.[41] Therefore, thermal conductivities and covalent bonds of the m-$Si_xGe_{3-x}N_4$ ($x = 0$, 1, 2, 3) become weaker following the above sequence.

Table 4. Values of density (in units g/cm^3), compressional, shear, and average sound velocities (in m/s) as well as Debye temperature (in K) for m-Si_3N_4, m-Si_2GeN_4, m-$SiGe_2N_4$, and m-Ge_3N_4..

Materials	ρ	v_p	v_s	v_m	Θ_D
m-Si_3N_4	3.070	5984	10082	6627	892
m-Si_2GeN_4	3.791	5066	8656	5618	744
m-$SiGe_2N_4$	4.442	4178	7854	4668	602
m-Ge_3N_4	4.994	3824	6694	4249	539

The elastic anisotropy analysis of a crystal is of great significance for understanding the mechanisms of material microcrack and durability in engineering science.[42] There are a variety of methods to quantity the anisotropy of a crystal structure, such as the universal anisotropic index A_U,[43] the percent compressibility of bulk and shear modulus factors (A_B and A_G).[44] According to the following equations, these mechanical anisotropic indexes mentioned above can be evaluated from

$$A_B = \frac{B_V - B_R}{B_V + B_R}, \tag{24}$$

$$A_G = \frac{G_V - G_R}{G_V + G_R}, \tag{25}$$

$$A^U = 5\frac{G_V}{G_R} + \frac{B_V}{B_R} - 6. \tag{26}$$

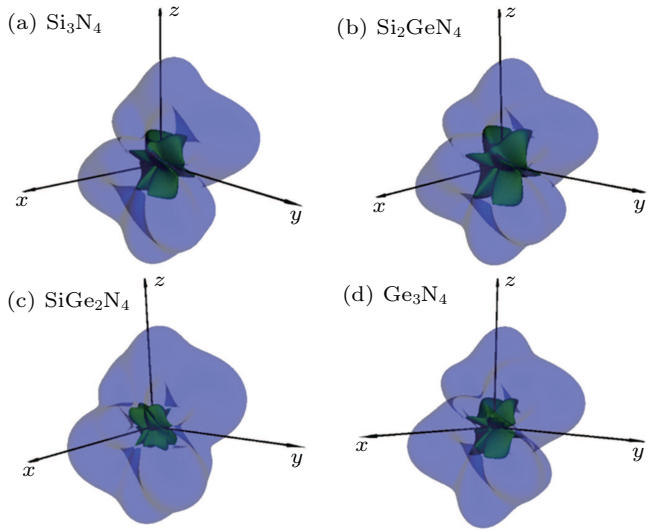


Fig. 3. (color online) 3D directional dependence of Poisson's ratio for (a) m-Si_3N_4, (b) m-Si_2GeN_4, (c) m-$SiGe_2N_4$, and (d) m-Ge_3N_4 at ambient pressure.

For isotropic crystals, the percentages of elastic anisotropy for bulk modulus A_B and shear modulus A_G, and universal anisotropic index A_U must be zero. The deviation from zero measures the anisotropy degree of crystal. The calculated anisotropy factors (A_B, A_G, and A_U) are presented in Table 3. It is obvious that the m-$Si_xGe_{3-x}N_4$ ($x = 0$, 1, 2, 3) are anisotropic. The value of A_G is much larger than A_B for

each crystal, indicating that the anisotropy of shear modulus is more conspicuous than that of bulk modulus. The values of the universal anisotropic index A_U are 0.968 for m-Si_3N_4, 0.905 for m-Si_2GeN_4, 2.557 for m-$SiGe_2N_4$, and 1.513 for m-Ge_3N_4, respectively. The anisotropy factors (A_B, A_G, and A_U) of m-$SiGe_2N_4$ are maxima, which indicates the anisotropy of m-$SiGe_2N_4$ is the largest among the m-$Si_xGe_{3-x}N_4$ ($x = 0$, 1, 2, 3).

Simultaneously, the elastic anisotropic m-$Si_xGe_{3-x}N_4$ ($x = 0$, 1, 2, 3) in Poisson's ratio, shear modulus and Young's modulus were investigated in the present work. The three-dimensional (3D) directional dependence and two-dimensional (2D) representation of anisotropy are calculated by utilizing the program of Elastic Anisotropy Measure (ELAM).[45] The vector direction (θ, ϕ) in the spherical coordinate system is used to describe the directional dependence of anisotropy, where θ (ϕ) represents the angle between the vector and the x-axis (z-axis) positive direction and they are expressed in radians. For an isotropic material, the 3D directional dependence would exhibit a spherical shape, while the deviation degree from the spherical shape reflects the content of anisotropy.[46]

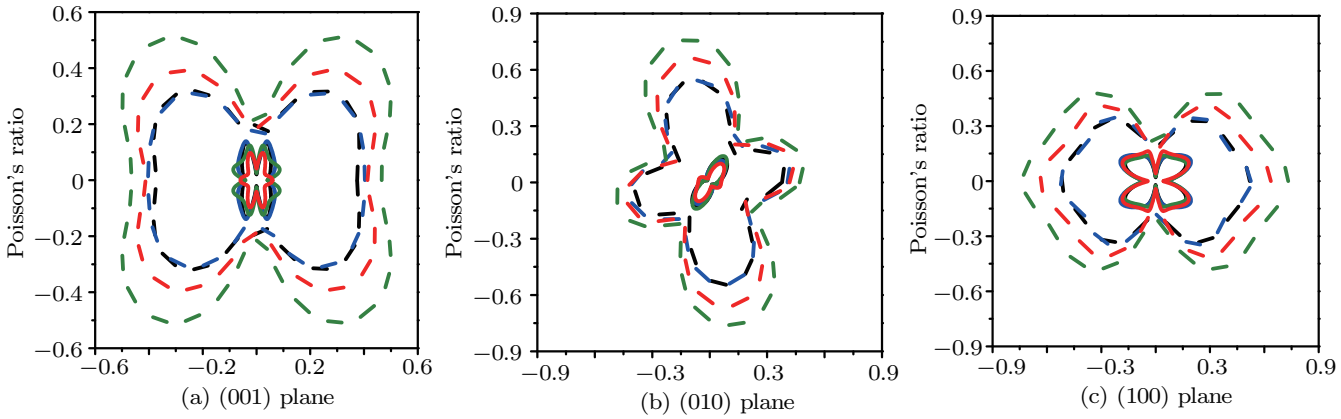


Fig. 4. (color online) 2D representations of Poisson's ratio in the (001), (010), and (100) planes for m-$Si_xGe_{3-x}N_4$ ($x = 0$, 1, 2, 3). The dash–dotted and solid lines represent the maximum and minimum values in the (001), (010), and (100) planes, respectively. The black, blue, green, and red lines denote the Poisson's ratios of m-Si_3N_4, m-Si_2GeN_4, m-$SiGe_2N_4$, and m-Ge_3N_4, respectively.

The calculated 3D directional dependence of Poisson's ratio and 2D representation in the (001), (010), and (100) planes for m-Si_3N_4, m-Si_2GeN_4, m-$SiGe_2N_4$, and m-Ge_3N_4 is shown in Figs. 3 and 4, respectively. It is evident that the 3D figures of the Poisson's ratio have a large degree of deviation in shape from the sphere, which implies that the Poisson's ratios of m-$Si_xGe_{3-x}N_4$ ($x = 0$, 1, 2, 3) are greatly anisotropic. The maximal (minimal) values of the Poisson's ratio for m-Si_3N_4, m-Si_2GeN_4, m-$SiGe_2N_4$, and m-Ge_3N_4 are 0.55 (0.02), 0.55 (0.03), 0.77 (0.02), and 0.67 (0.02) at 0 GPa. Following the sequence m-$Si_3N_4 \rightarrow m$-$Si_2GeN_4 \rightarrow m$-$SiGe_2N_4 \rightarrow m$-Ge_3N_4, the maximal and minimal Poisson's ratio directions are (3.14, 0.19), (3.14, 0.17), (0, 2.95), (3.14, 0.17) and (3.14, 0.89), (2.28, 0), (0, 2.38), (3.68, 1.35), respectively. It can be found that the maximal and minimal Poisson's ratio directions for m-Si_3N_4 and m-$SiGe_2N_4$ are both in the (010) plane. From Fig. 4, it can be seen that four compounds present the different degrees of anisotropy in Poisson's ratio in different planes. Following the above sequence, the ratios of v_{max}/v_{min} are $0.44/0.02 = 22$, $0.43/0.04 = 10.75$, $0.63/0.02 = 31.5$, and $0.52/0.04 = 13$ in the (001) plane, $0.55/0.02 = 27.5$, $0.55/0.03 = 18.33$, $0.77/0.02 = 35$, and $0.67/0.02 = 33.5$ in the (010) plane, and $0.52/0.02 = 26$, $0.53/0.04 = 13.25$, $0.48/0.03 = 16.33$, and $0.64/0.04 = 16$ in the (100) plane, respectively. Obviously, the anisotropy of the Poisson's ratio for m-$SiGe_2N_4$ is the largest one among m-$Si_xGe_{3-x}N_4$ ($x = 0$, 1, 2, 3).

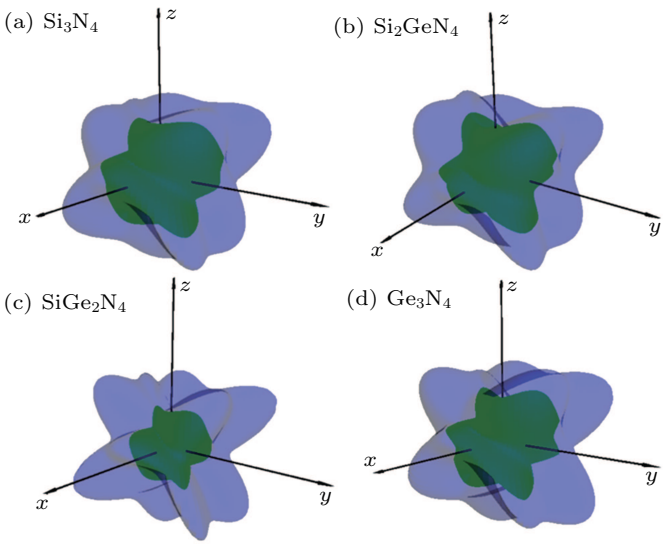


Fig. 5. (color online) 3D directional dependence of shear modulus for (a) m-Si_3N_4, (b) m-Si_2GeN_4, (c) m-$SiGe_2N_4$, and (d) m-Ge_3N_4 (d) at ambient pressure.

The shear moduli for all possible directions of shear strain are also calculated. The calculated 3D directional dependence

of shear modulus and 2D representations in the (001), (010), and (100) planes for the m-$Si_xGe_{3-x}N_4$ ($x = 0, 1, 2, 3$) are plotted in Figs. 5 and 6, respectively. The 3D figures reveal that the anisotropy of shear modulus is weak since the deviation degree from the sphere shape is small. The values of ratio G_{max}/G_{min} are as follows: $G_{max}/G_{min} = 188.54/63.24 = 2.98$ for m-Si_3N_4, $G_{max}/G_{min} = 164.45/57.71 = 2.85$ for m-Si_2GeN_4, $G_{max}/G_{min} = 173.95/29.99 = 5.8$ for m-$SiGe_2N_4$, $G_{max}/G_{min} = 132.65/36.25 = 3.66$ for m-Ge_3N_4 at 0 GPa. From Fig. 6, it is clear that the anisotropies of shear modulus in the (010) plane for the m-$Si_xGe_{3-x}N_4$ ($x = 0, 1, 2, 3$) are slightly larger than those in other planes. From m-Si_3N_4 to m-Ge_3N_4, the values of G_{max}/G_{min} are $150.31/63.24 = 2.38$, $129.87/57.71 = 2.25$, $118.83/29.98 = 3.96$, and $100.23/36.25 = 2.76$ in the (001) plane, $139.05/63.24 = 2.2$, $117.46/57.71 = 2.04$, $120.27/29.98 = 4.01$, and $97.68/36.25 = 2.69$ in the (010) plane, and $156.54/63.24 = 2.48$, $139.54/57.71 = 2.42$, $139.86/29.98 = 4.6$, and $119.49/36.25 = 3.29$ in the (100) plane, respectively. Consequently, m-$SiGe_2N_4$ exhibits larger anisotropy among m-$Si_xGe_{3-x}N_4$ ($x = 0, 1, 2, 3$).

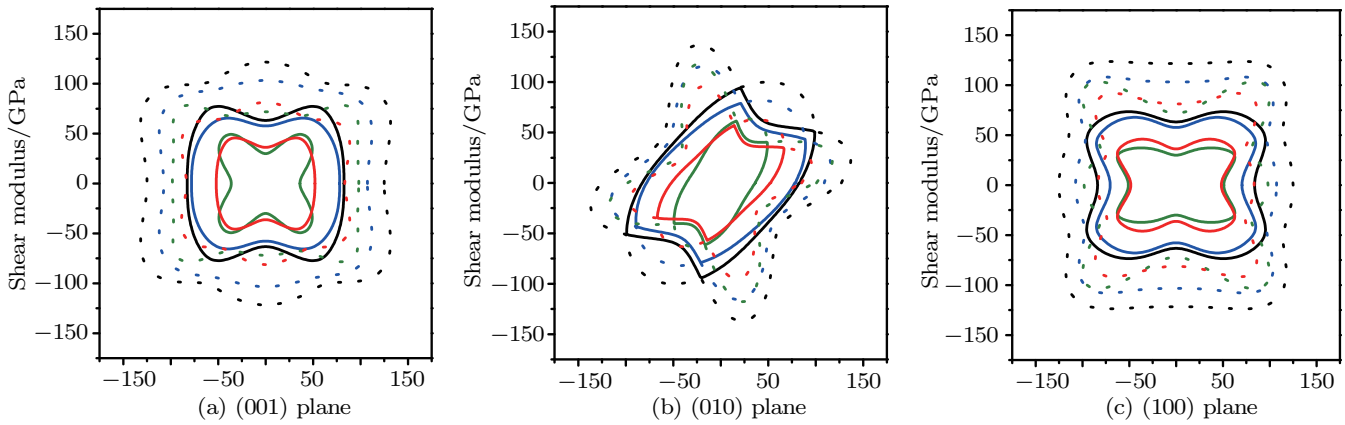


Fig. 6. (color online) 2D representations of shear modulus in the (001), (010) and (100) planes for m-$Si_xGe_{3-x}N_4$ ($x = 0, 1, 2, 3$). The dash dotted and solid lines represent the maximum and minimum values in the (001), (010), and (100) planes, respectively. The black, blue, green and red lines represent the Poisson's ratios of m-Si_3N_4, m-Si_2GeN_4, m-$SiGe_2N_4$, and m-Ge_3N_4, respectively.

The 3D directional dependencies of Young's modulus for m-$Si_xGe_{3-x}N_4$ ($x = 0, 1, 2, 3.$) are plotted in Fig. 7. It can be seen that the 3D figures of the m-Si_3N_4, m-Si_2GeN_4, m-$SiGe_2N_4$, and m-Ge_3N_4 have more or less deviations in shape from sphere along the x, y, z axes, which indicates that the Young's moduli of these compounds possess some kind of degree anisotropy. The values of ratio E_{max}/E_{min} are as follows: $E_{max}/E_{min} = 440/190 = 2.32$ for m-Si_3N_4, $E_{max}/E_{min} = 404/171 = 2.36$ for m-Si_2GeN_4, $E_{max}/E_{min} = 419/102 = 4.11$ for m-$SiGe_2N_4$, and $E_{max}/E_{min} = 335/114 = 2.94$ for m-Ge_3N_4 at 0 GPa. The calculated Young's moduli along different directions as well as in different planes for the m-Si_3N_4, m-Si_2GeN_4, m-$SiGe_2N_4$, and m-Ge_3N_4 are shown in Fig. 8. At first glance, the anisotropy of Young's modulus in (001) plane for m-$Si_xGe_{3-x}N_4$ ($x = 0, 1, 2, 3$) is similar to that in (100) plane but slightly larger than that in (010) planes. The values of E_{max}/E_{min} for m-Si_3N_4, m-Si_2GeN_4, m-$SiGe_2N_4$, and m-Ge_3N_4 are $440.27/193.73 = 2.28$, $404.44/181.34 = 2.23$, $418.92/106.91 = 3.92$, and $334.56/123.52 = 2.71$ in the (001) plane, $344.61/190.17 = 1.81$, $304.96/178.67 = 1.71$, $331.71/135.61 = 2.45$, and $267.23/120 = 2.23$ in the (010) plane, and $440.27/227.36 = 1.94$, $404.44/194.14 = 2.08$, $418.92/153.44 = 2.73$, and $334.56/139.31 = 2.4$ in the (100) plane, respectively. It can be noted that the maximum values of Young's modulus for m-Si_3N_4, m-Si_2GeN_4, m-$SiGe_2N_4$, and m-Ge_3N_4 in the (001) plane are the same as those in the (100) plane. A comparison of the values of E_{max}/E_{min} leads to a conclusion that the anisotropy of Young's modulus for m-$SiGe_2N_4$ is stronger among those of m-$Si_xGe_{3-x}N_4$ ($x = 0, 1, 2, 3$), which is consistent with the pervious conclusion.

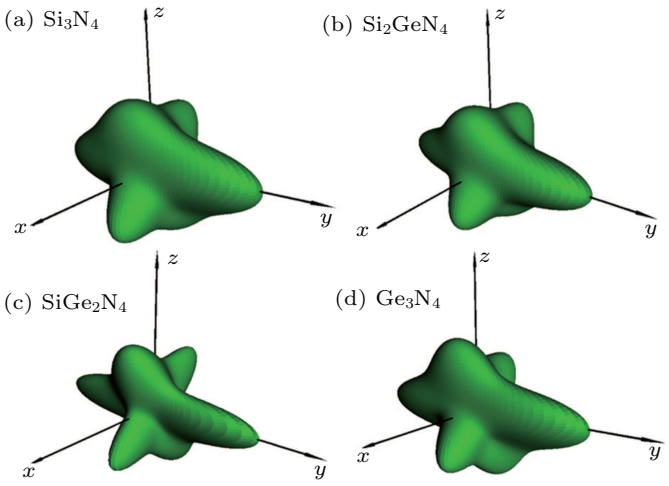


Fig. 7. (color online) 3D directional dependence of Young's modulus for (a) m-Si_3N_4, (b) m-Si_2GeN_4 , (c) m-$SiGe_2N_4$, and (d) m-Ge_3N_4 at ambient pressure.

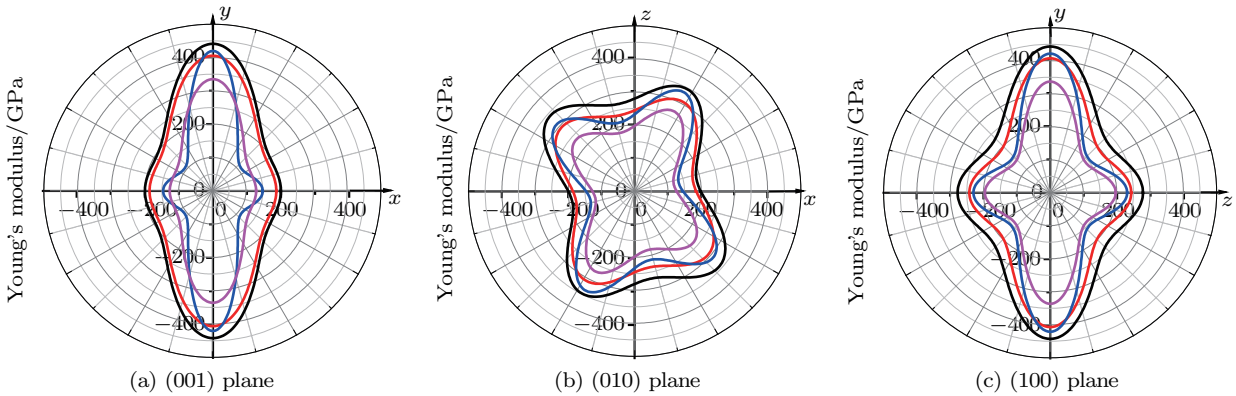


Fig. 8. (color online) 2D representations of Young's modulus in the (001), (010), and (100) planes for m-$Si_xGe_{3-x}N_4$ ($x = 0$, 1, 2, 3). The black, red, blue, and magenta lines represent the Poisson's ratios of m-Si_3N_4, m-Si_2GeN_4, m-$SiGe_2N_4$, and m-Ge_3N_4, respectively.

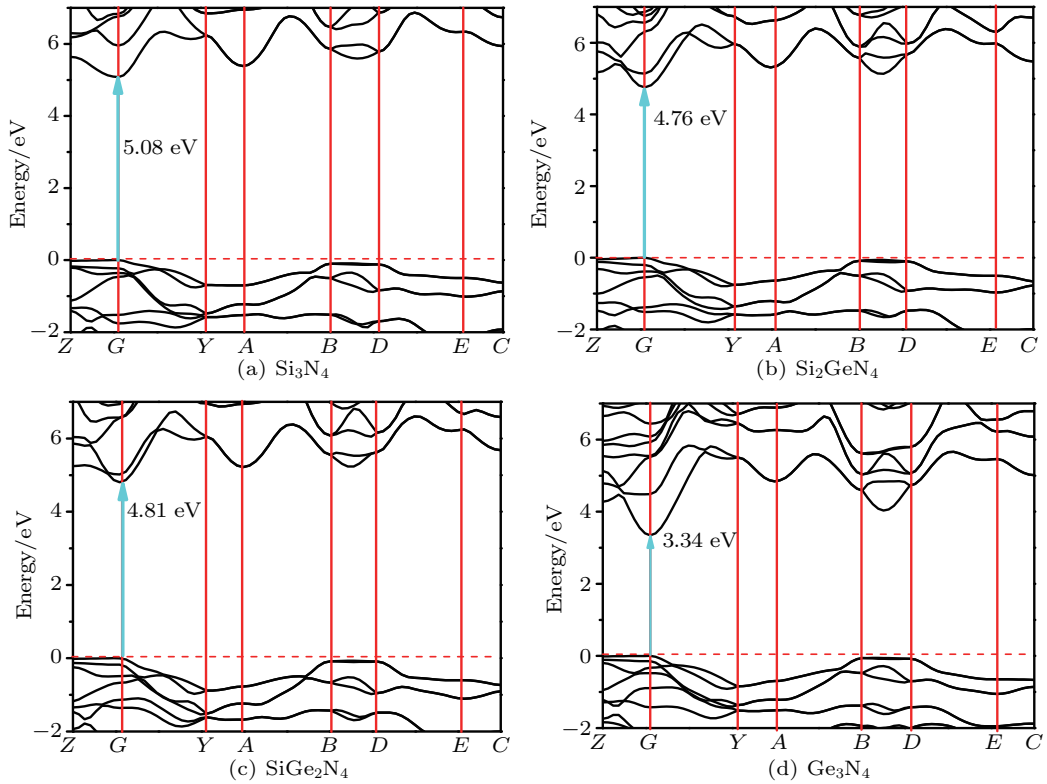


Fig. 9. (color online) Electronic band structures of (a) m-Si_3N_4, (b) m-Si_2GeN_4, (c) m-$SiGe_2N_4$, and (d) m-Ge_3N_4 with the HSE06 hybrid functional.

Physical properties can be measured in different directions. Various crystal properties, including the elastic modulus, hardness, fracture resistance, thermal expansion coefficient, thermal conductivity, resistivity, and electric displacement vector, have different levels of anisotropy. If a physical property is closely related to orientation, it is anisotropic. Why does this reverse phenomenon appear? This is because of the different atomic arrangements and different atomic positions, and different atoms have different lengths in different directions, resulting in the fact that the physical quantities along the different directions possess different values. For m-$Si_xGe_{3-x}N_4$ ($x = 0$, 1, 2, 3), they have a monoclinic symmetry that belongs to the *Cm* space group, the symmetry of the monoclinic system is very low. Young's modulus in Figs. 8(a) and 8(c) are symmetric with respect to the *xy* plane and *yz* plane, respectively, but in Fig. 8(b), the symmetry axis are not along the *xz* plane. And both the Poisson's ratio, and the shear modulus have the same situation as Young's modulus. That is to say, the symmetries of Young's modulus, Poisson's ratio, and shear modulus in the *xz* plane are lower than in the *xy* plane and *yz* plane.

The electronic band structure reflects the law of the electron motion in a solid and determines the fundamental physical and chemical properties of material. The band structures of m-Si_3N_4, m-Si_2GeN_4, m-$SiGe_2N_4$, and m-Ge_3N_4 along some high symmetry directions of the Brillouin zone are calculated with HSE06 functional at ambient pressure, and the results are shown in Fig. 9. The horizontal red dash line designates zero

energy representing the Fermi lever (E_F). At first glance, it appears that the four band structures are very similar. The major differences are in the width of band gap and conduction band minimum. From Fig. 9, it is clear that the valance band maximum (VBM) and the conduction band minimum (CBM) of m-$Si_xGe_{3-x}N_4$ ($x = 0$, 1, 2, 3) are both located at G point. Therefore, m-Si_3N_4, m-Si_2GeN_4, m-$SiGe_2N_4$, and m-Ge_3N_4 are direct semiconductors with band gaps of 5.08 eV, 4.76 eV, 4.81 eV, and 3.34 eV, respectively. It should be noted that no experimental dataare available to verify the band gaps of these compounds. All the previous results are obtained via theoretical methods, which need to be verified experimentally in future.

To further investigate the natures of the electronic band structure for m-Si_3N_4, m-Si_2GeN_4, m-$SiGe_2N_4$, and m-Ge_3N_4, the partial densities of states (PDOSs) are calculated as shown in Fig. 10. It is obvious that PDOSs of m-$Si_xGe_{3-x}N_4$ ($x = 0$, 1, 2, 3) look similar on a gross scale since they have the same crystal structure and Si and Ge are isoelectronic elements. The densities of electronic states are separated into three regions by the gaps. The first region is in the energy range between -20 eV and -15 eV, the second region is between -10 eV and Fermi energy (E_F), and the last region ranges from 5 eV to 11 eV in the conduction band. For m-Si_3N_4 (m-Ge_3N_4), the first region is mainly for N-s states with admixture from Si (Ge)-s/p states, the second region mainly involves N-p states with significant contributions from Si (Ge)-s states (between 10 eV to -7.5 eV) and Si (Ge)-p states (from -7.5 eV to E_F), and the third region mainly contains Si (Ge)-p states and a mixture of Si (Ge)-s states and N-s/p states. For m-Si_2GeN_4 and m-$SiGe_2N_4$, the first region mainly contains N-s states with a mixture of Si- and Ge-s/p states, the second region mainly involes N-p states with significant contributions from Si- and Ge-s/p states, and the third region mainly covers Si/Ge-p states and a mixture of Si (Ge)-s states and N-s/p states.

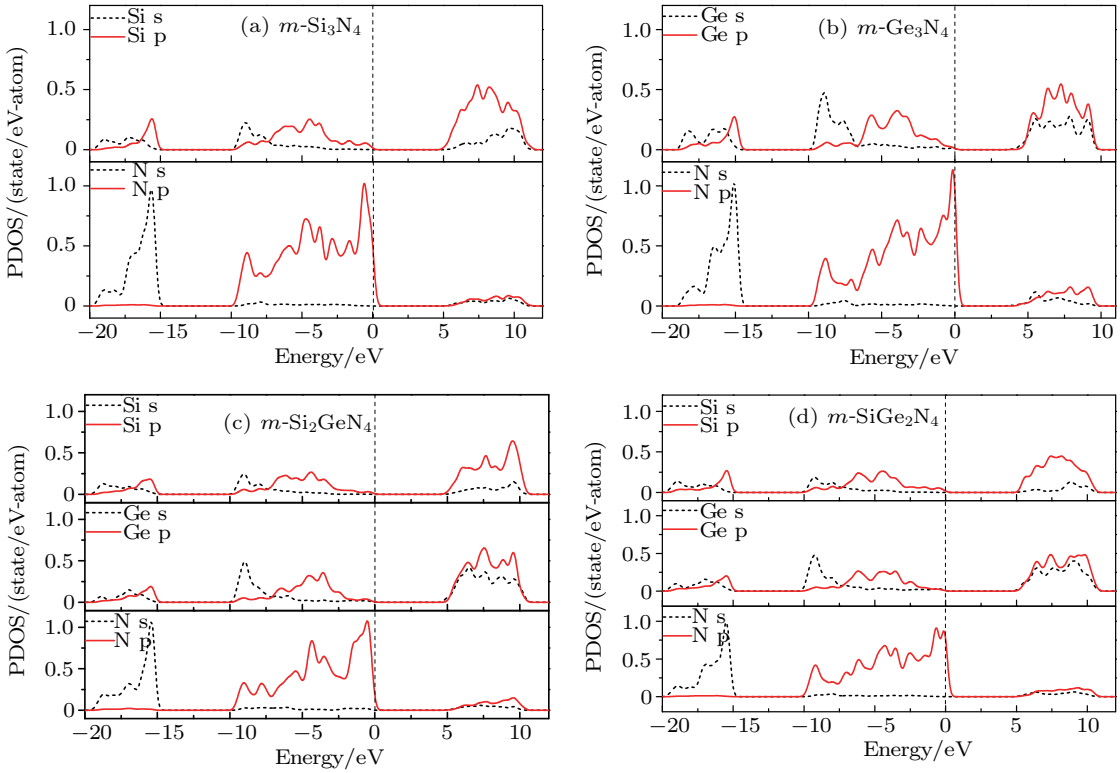


Fig. 10. (color online) Comparisons of total density of states and partial density of states for m-Si_3N_4, m-Si_2GeN_4, m-$SiGe_2N_4$, and m-Ge_3N_4. The black/dash and red/solid curves represent s states and p states of silicon, germanium, and nitrogen atoms, respectively.

4. Conclusions

The structural, electronic, elastic, and anisotropic properties of the monoclinic phases of m-Si_3N4, m-Si_2GeN_4, m-$SiGe_2N_4$, and m-Ge_3N_4 are investigated systemically in this work. The calculated lattice constants, elastic constants and elastic moduli of m-Si_3N_4 and m-Ge_3N_4 are in good consistence with previous theoretical results. The elastic constants of m-$Si_xGe_{3-x}N_4$ ($x = 1$, 2) satisfy the stability criteria, which indicates that they are mechanically stable. According to the analyses of the obtained values of Poisson's ratio v and B/G, it is found that only m-$SiGe_2N_4$ is ductile in nature. The densities of m-$Si_xGe_{3-x}N_4$ ($x = 0$, 1, 2, 3) increase whereas the Debye temperature Θ_D and the sound velocities decrease with increasing the composition of germanium. The detailed analyses of the anisotropy manifest that the m-$Si_xGe_{3-x}N_4$ ($x = 0$, 1, 2, 3) exhibit lager anisotropy and the anisotropy of m-$SiGe_2N_4$ is the largest among the m-$Si_xGe_{3-x}N_4$ ($x = 0$, 1, 2, 3). The calculated band structures show that they are all direct semi-

conductors with band gaps of 5.08 eV, 4.76 eV, 4.81 eV, and 3.34 eV, respectively.

Acknowledgment

The authors thank Q Y Fan (School of Microelectronics, Xidian University) for being allowed to use the CASTEP code in Materials Studio.

References

[1] Jack K H 1976 *J. Mater. Sci.* **11** 1135
[2] Clarke D R, Lange F F and Schnittgrund G D 1982 *J. Am. Ceram. Soc.* **65** c51
[3] Riley F L 2000 *J. Am. Ceram. Soc.* **83** 245
[4] Xu B, Dong J J, McMillan P F, Shebanova O and Salamat A 2011 *Phys. Rev. B* **84** 014113
[5] Ching W Y, Mo S D, Ouyang L Z, Rulis P, Tanaka I and Yoshiya M 2002 *J. Am. Ceram. Soc.* **85** 75
[6] Yu B H and Chen D 2013 *J. Alloys Compd.* **581** 747
[7] Yu B H and Chen D 2012 *Physica B* **407** 4660
[8] Wang H, Chen Y, Kaneta Y and Iwata S 2006 *J. Phys.: Condens. Mater.* **18** 10663
[9] Ching W Y, Mo S D and Ouyang L 2001 *Phys. Rev. B* **63** 245110
[10] Moakafi M, Khenata R, Bouhemadou A, Benkhettou N, Rached D, Reshak A and Elastic H 2009 *Phys. Lett. A* **373** 2393
[11] Bouhemadou A, Al-Douri Y, Khenata R and Haddadi K 2009 *Eur. Phys. J. B* **71** 185
[12] Zhang X Y, Chen Z W, Du H J, Ma M Z, He J L, Tian Y J and Liu R P 2008 *J. Appl. Phys.* **103** 083533
[13] Cui L, Hu M, Wang Q Q, Xu B, Yu D L, Liu Z Y and He J L 2015 *J. Solid State Chem.* **228** 20
[14] Cang Y P, Chen D, Yang F and Yang H M 2016 *Chem. J. Chin. Univer.* **37** 674
[15] Fan Q Y, Chai C C, Wei Q, Zhou P K and Yang Y T 2016 *AIP Adv.* **6** 085207
[16] Chen D, Cheng K and Qi B Y 2017 *Chin. Phys. B* **26** 046303
[17] Hohenberg P and Kohn W 1964 *Phys. Rev.* **136** B864
[18] Kohn W and Sham L J 1965 *Phy. Rev.* **137** 1697
[19] Clark S.J, Segall M D, Pickard C J, Hasnip P J, Probert M I J, Refson K and Payne M C 2005 *Z. Krist.-Cryst. Mater.* **220** 567
[20] Perdew J P, Burke K and Ernzerhof M 1996 *Phys. Rev. Lett.* **77** 3865
[21] Perdew J P, Ruzsinszky A, Csonka G I, Vydrov O A, Scuseria G E, Constantin L A, Zhou X L and Burke K 2008 *Phys. Rev. Lett.* **100** 136406
[22] Ceperley D M and Alder B J 1980 *Phys. Rev. Lett.* **45** 566
[23] Perdew J P, Mcmullen E R and Zunger A 1981 *Phys. Rev. A* **23** 2785
[24] Pfrommer B G, Côté M, Louie S G and Cohen M L 1997 *J. Comput. Phys.* **131** 233
[25] Vanderbilt D 1990 *Phys. Rev. B* **41** 7892
[26] Monkhorst H J and Pack J D 1976 *Phys. Rev. B* **13** 5188
[27] Krukau A V, Vydrov O A, Izmaylov A F and Scuseria G E 2006 *J Chem. Phys.* **125** 224106
[28] Nye J F 1985 *Physical properties of crystals* (New York: Oxford university press)
[29] Hao X P and Cui H L 2014 *J. Korean Phys. Soc.* **65** 45
[30] Wu Z J, Zhao E J, Xiang H P, Hao X F, Liu X J and Meng J 2007 *Phys. Rev. B* **76** 054115
[31] Reuss A 1929 *Z. Angew. Math. Mech.* **9** 49
[32] Vaitheeswaran G, Kanchana V, Kumar R S, Cornelius A L, Nicol M F, Savane A, Delin A and Johansson B 2007 *Phys. Rev. B* **76** 014107
[33] Liu Y, Hu W C, Li D J, Zeng X Q and Xu C S 2013 *Phys. Scr.* **88** 045302
[34] Duan Y H, Sun Y, Peng M J and Zhou S G 2014 *J. Alloys Compd.* **595** 14
[35] Pugh S F 1954 *Philos. Mag.* **45** 823
[36] Anderson O L 1963 *J. Phys. Chem. Solids.* **24** 909
[37] Fan Q Y, Chai C C, Wei Q, Yan H Y, Zhao Y B, Yang Y T, Yu X H, Liu Y, Xing M J, Zhang J.Q and Yao R H 2015 *J. Appl. Phys.* **118** 185704.
[38] Duan Y H, Huang B, Sun Y, Peng M J and Zhou S G 2014 *J. Alloys Compd.* **590** 50
[39] Hu W C, Liu Y, Li D J, Zeng X Q and Xu C S 2014 *Comput. Mater. Sci.* **83** 27
[40] Li J, Zhang M and Luo X 2013 *J. Alloys Compd.* **556** 214
[41] Pan Y, Zheng W T, Guan W M, Zhang K H and Fan X F 2013 *J. Solid State Chem.* **207** 29
[42] Duan Y H, Sun Y, Peng M J and Zhou S G 2014 *J. Alloys Compd.* **595** 14
[43] Ranganathan S I and Ostoja-Starzewski M 2008 *Phys. Rev. Lett.* **101** 055504
[44] Fan Q Y, Wei Q, Yan H Y, Zhang M G, Zhang Z X, Zhang J Q and Zhang D Y 2014 *Comput. Mater. Sci.* **85** 80
[45] Marmier A, Lethbridge Z A D, Walton R I, Smith C W, Parker S C and Evans K E 2010 *Comput. Phys. Commun.* **181** 2102
[46] Hu W C, Liu Y, Li D J, Zeng X Q and Xu C S 2014 *Comput. Mater. Sci.* **83** 27